The Astrophysical Journal, 818:78 (11pp), 2016 February 10 doi:10.3847/0004-637X/818/1/78

REACTION RATES OF ^{64}Ge$(p,\gamma)^{65}$As AND ^{65}As$(p,\gamma)^{66}$Se AND THE EXTENT OF NUCLEOSYNTHESIS IN TYPE I X-RAY BURSTS

Y. H. Lam[1], J. J. He[1], A. Parikh[2,3], H. Schatz[4], B. A. Brown[4], M. Wang[1], B. Guo[5], Y. H. Zhang[1], X. H. Zhou[1], and H. S. Xu[1]
[1] Key Laboratory of High Precision Nuclear Spectroscopy, Institute of Modern Physics, Chinese Academy of Sciences, Lanzhou 730000, China; jianjunhe@impcas.ac.cn
[2] Departament de Física i Enginyeria Nuclear, EUETIB, Universitat Politècnica de Catalunya, Barcelona E-08036, Spain; anuj.r.parikh@upc.edu
[3] Institut d'Estudis Espacials de Catalunya, Barcelona E-08034, Spain
[4] Department of Physics and Astronomy and National Superconducting Cyclotron Laboratory, Michigan State University, East Lansing, Michigan 48824-1321, USA; schatz@nscl.msu.edu
[5] China Institute of Atomic Energy, P.O. Box 275(10), Beijing 102413, China
Received 2015 May 14; accepted 2015 December 30; published 2016 February 9

ABSTRACT

The extent of nucleosynthesis in models of type I X-ray bursts (XRBs) and the associated impact on the energy released in these explosive events are sensitive to nuclear masses and reaction rates around the ^{64}Ge waiting point. Using the well known mass of ^{64}Ge, the recently measured ^{65}As mass, and large-scale shell model calculations, we have determined new thermonuclear rates of the ^{64}Ge$(p,\gamma)^{65}$As and ^{65}As$(p,\gamma)^{66}$Se reactions with reliable uncertainties. The new reaction rates differ significantly from previously published rates. Using the new data, we analyze the impact of the new rates and the remaining nuclear physics uncertainties on the ^{64}Ge waiting point in a number of representative one-zone XRB models. We find that in contrast to previous work, when all relevant uncertainties are considered, a strong ^{64}Ge *rp*-process waiting point cannot be ruled out. The nuclear physics uncertainties strongly affect XRB model predictions of the synthesis of ^{64}Zn, the synthesis of nuclei beyond $A = 64$, the energy generation, and the burst light curve. We also identify key nuclear uncertainties that need to be addressed to determine the role of the ^{64}Ge waiting point in XRBs. These include the remaining uncertainty in the ^{65}As mass, the uncertainty of the ^{66}Se mass, and the remaining uncertainty in the ^{65}As$(p,\gamma)^{66}$Se reaction rate, which mainly originates from uncertain resonance energies.

Key words: nuclear reactions, nucleosynthesis, abundances – stars: neutron – X-rays: bursts

1. INTRODUCTION

A type I X-ray burst (XRB) arises from a thermonuclear runaway in the accreted envelope of a neutron star in a close binary star system (for reviews, see, e.g., Lewin et al. 1993; Schatz et al. 1998; Strohmayer & Bildsten 2006; Parikh et al. 2013). Roughly 100 bursting systems have been discovered to date, with light curves exhibiting peak luminosities of $L_{\rm peak} \approx 10^4$–$10^5 L_\odot$ and timescales of 10–100 s. During an XRB, models predict that a H/He-rich accreted envelope may become strongly enriched in heavier nuclei through the αp-process and the *rp*-process (Wallace & Woosley 1981; Schatz et al. 1998). These two processes involve α-particle-induced or proton-capture reactions on stable and radioactive nuclei, interrupted by occasional β-decays. When the *rp*-process approaches the proton drip line, successive capture of protons by nuclei is inhibited by a strong reverse photodisintegration reaction rate. The competition between the rate of proton capture and the rate of β-decay at these "waiting points" (e.g., ^{60}Zn, ^{64}Ge, and ^{68}Se) determines the extent of the synthesis of heavier mass nuclei during the burst (Schatz et al. 1998). Peak temperatures during the thermonuclear runaway may approach or exceed 1 GK, resulting in the synthesis of nuclei up to a mass of $A \approx 100$ (Schatz et al. 2001; Elomaa et al. 2009). Model predictions depend, however, on astrophysical parameters such as accretion rate, the composition of the accreted material, and the neutron star surface gravity, as well as on nuclear physics quantities such as nuclear masses and reaction rates.

The ^{64}Ge$(p,\gamma)^{65}$As and ^{65}As$(p,\gamma)^{66}$Se reactions have been demonstrated to have a significant impact on nucleosynthesis during XRBs. (See Parikh et al. (2014) for a recent review of the impact of nuclear physics uncertainties on predicted yields and light curves from XRB models.) Direct measurements of these reactions at the relevant energies in XRBs are not yet possible due to the lack of sufficiently intense radioactive ^{64}Ge and ^{65}As beams. Moreover, due to the unknown mass of ^{66}Se and the lack of nuclear structure information for states within ≈1–2 MeV of the ^{64}Ge+p and the (theoretical) ^{65}As+p energy thresholds in ^{65}As and ^{66}Se, respectively, it is not possible to estimate rates for these reactions based on experimental nuclear structure data. As a result, XRB models use ^{64}Ge$(p,\gamma)^{65}$As and ^{65}As$(p,\gamma)^{66}$Se thermonuclear rates derived from theoretical calculations. Using such models, it has been demonstrated that varying the ^{65}As$(p,\gamma)^{66}$Se rate by a factor of 10 at the relevant temperatures affects the calculated abundances of nuclei between $A \approx 65$–100 by factors as large as about five (Parikh et al. 2008). For ^{64}Ge$(p,\gamma)^{65}$As, models have illustrated the importance of the Q-value (or proton separation energy $S_{\rm p}$) adopted for this reaction, with variations by ±300 keV affecting final calculated abundances between $A \approx 65$–100 by factors as large as about five (Parikh et al. 2008, 2009). In addition, the effective *rp*-process lifetime of the waiting-point nucleus ^{64}Ge was investigated by Schatz (2006) based on the estimated proton separation energies of $S_{\rm p}(^{65}{\rm As}) = -0.36 \pm 0.15$ MeV and $S_{\rm p}(^{66}{\rm Se}) = 2.43 \pm 0.18$ MeV, derived from Coulomb mass shift calculations (Brown et al. 2002). It was found that the effective lifetime of ^{64}Ge for a given temperature and proton density is mainly determined by the $S_{\rm p}$ values of ^{65}As and ^{66}Se and the proton capture rate on ^{65}As.

Recently, precise mass measurements of nuclei along the *rp*-process path have become available. The mass of ^{64}Ge has been measured at the Canadian Penning Trap at the Argonne

National Laboratory (Clark et al. 2007) and the LEBIT Penning Trap facility at Michigan State University (Schury et al. 2007). More recently, the mass of ^{65}As has been measured at the HIRFL-CSR (Cooler-Storage Ring at the Heavy Ion Research Facility in Lanzhou; Xia et al. 2002) using IMS (Isochronous Mass Spectrometry). The measurements can be combined to obtain an experimental proton separation energy for ^{65}As of $S_p = -90 \pm 85$ keV (Tu et al. 2011), where the uncertainty is dominated by the uncertainty in the ^{65}As mass. The mass of ^{66}Se is not known experimentally. The extrapolated value predicted by AME2012 (Wang et al. 2012) results in $S_p(^{66}\mathrm{Se}) = 1720 \pm 310$ keV. With the new mass of ^{65}As, XRB model calculations (Tu et al. 2011) suggested that ^{64}Ge may not be a significant *rp*-process waiting point, contrary to previous expectations (Schatz et al. 1998; Woosley et al. 2004; Fisker et al. 2008; Parikh et al. 2009; José et al. 2010). We revisit this question here using our new nuclear reaction rates.

Thermonuclear ^{64}Ge(p,γ) and ^{65}As(p,γ) reaction rates were first estimated by Van Wormer et al. (1994) based entirely on the properties of the mirror nuclei ^{65}Ge and ^{66}Ge, respectively. S_p values of ^{65}As and ^{66}Se were estimated to be 0.169 MeV and 1.909 MeV, respectively. Later on, both rates were calculated (Rauscher & Thielemann 2000) with the statistical Hauser-Feshbach formalism (NON-SMOKER; Rauscher & Thielemann 1998) using the masses of ^{65}As and ^{66}Se predicted by the finite-range droplet (FRDM; Möller et al. 1995) and ETSFIQ (Pearson et al. 1996) mass models. Recently, the statistical model calculations have been updated using new predictions for the ^{65}As and ^{66}Se proton separation energies (see JINA REACLIB[6] Cyburt et al. 2010). The predicted rates differ from one another by up to several orders of magnitude over typical XRB temperatures. Moreover, the reliability of statistical model calculations for these rates is questionable due to the low compound nucleus level densities, especially for ^{64}Ge(p,γ), but also for ^{65}As(p,γ).

In this work, we refer to previously available rates using the nomenclature adopted in the JINA REACLIB database. The *laur* rate refers to the rate estimated by Van Wormer et al. (1994); the *rath* rate was calculated by Rauscher & Thielemann (2000). The *rath, thra,* and *rpsm*rates are the statistical model calculations with FRDM, ETSFIQ, as well as Audi & Wapstra (1995) estimated masses, respectively. The recent *ths8* rate is from Cyburt et al. (2010).

Here we determine new thermonuclear ^{64}Ge(p,γ)^{65}As and ^{65}As(p,γ)^{66}Se reaction rates using the updated S_p values of ^{65}As and ^{66}Se together with new nuclear structure information from large-scale shell model calculations. Using the new data, we fully characterize the nuclear physics uncertainties that affect the *rp*-process through ^{64}Ge and reexamine the question of the ^{64}Ge waiting point.

2. REACTION RATE CALCULATIONS

The total thermonuclear proton capture reaction rate consists of the sum of resonant- and direct-capture (DC) on ground state and thermally excited states in the target nucleus, weighted with their individual population factors (Fowler & Hoyle 1964; Rolfs & Rodney 1988). It can be calculated by the following equation.

$$N_A\langle\sigma v\rangle = \sum_i (N_A\langle\sigma v\rangle_r^i + N_A\langle\sigma v\rangle_{\mathrm{DC}}^i)\frac{(2J_i+1)e^{-E_i/kT}}{\sum_n (2J_n+1)e^{-E_n/kT}} \quad (1)$$

with the parameters defined by Schatz et al. (2005).

2.1. Resonant Rates

For isolated narrow resonances, the resonant reaction rate for capture on a nucleus in an initial state i, $N_A\langle\sigma v\rangle_r^i$, can be calculated as a sum over all relevant compound nucleus states j above the proton threshold (Rolfs & Rodney 1988; Iliadis 2007). It can be expressed by the following equation (Schatz et al. 2005).

$$N_A\langle\sigma v\rangle_r^i = 1.54 \times 10^{11}(\mu T_9)^{-3/2} \times \sum_j \omega\gamma_{ij} \times \exp\left(-\frac{11.605E_{ij}}{T_9}\right)[\mathrm{cm^3\ s^{-1}\ mol^{-1}}], \quad (2)$$

where the resonance energy in the center-of-mass system, $E_{ij} = E_j - S_p - E_i$, is calculated from the excitation energies of the initial E_i and compound nucleus E_j state. For the ground-state capture, the resonance energy is represented by $E_r^i = E_x^j - S_p$. T_9 is the temperature in Giga Kelvin (GK) and μ is the reduced mass of the entrance channel in atomic mass units ($\mu = A_T/(1+A_T)$, with A_T as the target mass number). In Equation (2), the resonance energy and strength are in units of MeV. The resonance strength $\omega\gamma$ is defined by

$$\omega\gamma_{ij} = \frac{2J_j+1}{2(2J_i+1)}\frac{\Gamma_p^{ij}\times\Gamma_\gamma^j}{\Gamma_{\mathrm{total}}^j}. \quad (3)$$

where J_i is the target spin and J_j, Γ_p^{ij}, Γ_γ^j, and $\Gamma_{\mathrm{total}}^j$ are spin, proton decay width, γ-decay width, and total width of the compound nucleus state j, respectively. The total width is given by $\Gamma_{\mathrm{total}}^j = \Gamma_\gamma^j + \sum_i \Gamma_p^{ij}$, because other decay channels are closed (Audi et al. 2012) in the excitation energy range considered in this work.

The proton width can be estimated by the following equation,

$$\Gamma_p = \sum_{nlj} C^2S(nlj)\,\Gamma_{\mathrm{sp}}(nlj), \quad (4)$$

where $C^2S(nlj)$ denotes a proton-transfer spectroscopic factor, while Γ_{sp} is a single-proton width for capture of a proton on an (nlj) quantum orbital. The Γ_{sp} are obtained from proton scattering cross sections calculated with a Woods–Saxon potential (Richter et al. 2011; Brown 2014). Alternatively, the proton partial widths may also be calculated by the following expression (Van Wormer et al. 1994; Herndl et al. 1995),

$$\Gamma_p = \frac{3\hbar^2}{\mu R^2}P_\ell(E)\,C^2S. \quad (5)$$

Here, $R = r_0 \times (1+A_T)^{1/3}$ fm (with $r_0 = 1.25$ fm) is the nuclear channel radius. The Coulomb penetration factor P_ℓ is

[6] http://groups.nscl.msu.edu/jina/reaclib/db

Table 1
Properties of ^{65}As for the Ground-state Capture Utilized in the Present ^{64}Ge$(p,\gamma)^{65}$As Resonant Rate Calculation

J_i^{π} [a]	E_x (MeV)			E_r (MeV)[d]	nlj	C^2S	Γ_p (eV)	Γ_γ (eV)	$\omega\gamma$ (eV)
	$E_x^{\exp}$ [a]	E_x^{theo} [b]	$E_x(^{65}\text{Ge})$[c]						
$3/2_1^-$	0.000	0.000	0.000	0.090	$2p_{3/2}$	0.196	1.19×10^{-34}	0.00	0.00
$5/2_1^-$[e]	0.187(3)	0.103	0.111	0.277	$1f_{5/2}$	0.533	8.19×10^{-17}	5.11×10^{-7}	2.46×10^{-16}
$5/2_2^-$	⋯	0.501	0.605	0.591	$1f_{5/2}$	0.010	3.76×10^{-10}	4.73×10^{-5}	1.13×10^{-9}
$5/2_3^-$	⋯	0.863	⋯	0.953	$1f_{5/2}$	0.014	1.64×10^{-6}	4.24×10^{-4}	4.89×10^{-6}
$7/2_1^-$	⋯	0.947	0.890	1.037	$1f_{7/2}$	0.013	1.28×10^{-5}	2.43×10^{-4}	4.88×10^{-5}
$7/2_2^-$[f]	⋯	1.070	1.155	1.160	$1f_{7/2}$	0.002	8.50×10^{-6}	2.11×10^{-4}	3.27×10^{-5}

Notes. The energy levels in the mirror nucleus ^{65}Ge are listed in the fourth column for comparison.
[a] Measured by Obertelli et al. (2011).
[b] Calculated by the present shell model.
[c] Compiled by Browne & Tuli (2010).
[d] Calculated by $E_r = E_x - S_p$ with $S_p = -0.09$ MeV (Tu et al. 2011).
[e] Calculated E_r and Γ_p based on the experimental value of $E_x = 0.187$ MeV for this state.
[f] Negligible contribution to the rate for temperatures up to 2 GK.

given by

$$P_\ell(E) = \frac{kR}{F_\ell^2(E) + G_\ell^2(E)}, \quad (6)$$

where $k = \sqrt{2\mu E}/\hbar$ is the wave number with energy E in the center-of-mass (c.m.) system; F_ℓ and G_ℓ are the regular and irregular Coulomb functions, respectively. The proton widths given by these two methods (i.e., by Equations (4) and (5)) agree well with each other, with a maximum difference of about 35%.

The key ingredients necessary to estimate the resonant ^{64}Ge (p,γ) and ^{65}As(p,γ) rates are energy levels in ^{65}As and ^{66}Se, proton-transfer spectroscopic factors, and proton and gamma-ray partial widths. For ^{65}As, only a single level has been observed at $E_x = 187(3)$ keV (Obertelli et al. 2011). For ^{66}Se, one level has been confirmed at $E_x = 929(7)$ keV, and indications for two other levels at 2064(3) keV and 3520 (4) keV have been reported, with tentative assignments of (4^+) and (6^+), respectively (Obertelli et al. 2011; Ruotsalainen et al. 2013). There are no more experimental data available for these two nuclei. In this work, we have calculated the energy levels, spectroscopic factors and gamma widths within the framework of a large-scale shell model, without truncation, using the shell model code NuShellX@MSU (Brown & Rae 2014). The effective interaction GXPF1a (Honma et al. 2004, 2005) has been utilized for these two *pf*-shell nuclei.

The γ widths, Γ_γ, have been calculated from the electromagnetic reduced transition probabilities $B(J_i \rightarrow J_f; L)$, which carry the nuclear structure information of the resonant states and the final bound states (Brussaard & Glaudemans 1977). The reduced transition rates are computed within the shell model. Most of the transitions in this work are of $M1$ and $E2$ types. The relations are (Herndl et al. 1995):

$$\Gamma_{E2}[\text{eV}] = 8.13 \times 10^{-7} E_\gamma^5[\text{MeV}] B(E2)[\text{e}^2\text{fm}^4], \quad (7)$$

and

$$\Gamma_{M1}[\text{eV}] = 1.16 \times 10^{-2} E_\gamma^3[\text{MeV}] B(M1)[\mu_N^2]. \quad (8)$$

The $B(E2)$ values have been obtained from empirical effective charges, $e_p = 1.5e$, $e_n = 0.5e$, whereas the $B(M1)$ values have been obtained with a four-parameter set of empirical g-factors, i.e., $g_p^s = 5.586$, $g_n^s = -3.826$ and $g_p^l = 1$, $g_n^l = 0$ (Honma et al. 2004).

In addition, we have also included proton resonant captures on the thermally excited target states. Since the first-excited state in ^{64}Ge is quite high ($E_x = 902$ keV), thermal excitation can be neglected for typical XRB temperatures. For the ^{65}As$(p,\gamma)^{66}$Se rate, we included proton capture on the first four thermally excited states of ^{65}As (i.e., on the 0.187, 0.501, 0.863, and 0.947 MeV states listed in Table 1). Capture on thermally excited states contributes at most 38% to the total capture rate at 2 GK (Y. H. Lam et al. 2016, in preparation). The properties of ^{65}As and ^{66}Se for the ground-state captures are summarized in Tables 1 and 2, respectively. In addition, the properties of ^{66}Se for the first-excited-state capture (the major thermally excited-state contribution) are summarized in Table 3.

Peak temperatures in recent hydrodynamic XRB models have approached 1.5–2 GK (Woosley et al. 2004; José et al. 2010). At such temperatures, resonant rates for the ^{64}Ge (p,γ) and ^{65}As(p,γ) reactions are expected to be dominated by levels with $E_r \leqslant 2.5$ MeV, i.e., Gamow energy Rolfs & Rodney 1988). This means that excitation energy regions of up to $E_x \leqslant 2.5$ MeV for ^{65}As, and up to $E_x \leqslant 4.2$ MeV for ^{66}Se should be considered in the resonant rate calculations for ^{64}Ge (p,γ) and ^{65}As(p,γ), respectively. In the present shell model calculations, the maximum excitation energies considered for ^{65}As and ^{66}Se are 1.07 MeV and 3.50 MeV, respectively (see Tables 1 and 2). For ^{64}Ge(p,γ) only resonances up to $E_r = 1.035$ MeV contribute significantly to the reaction rate up to 2 GK; for ^{65}As(p,γ) only five resonances (at $E_r = 0.333$, 0.557, 0.754, 0.836, and 1.061 MeV) dominate the total resonant rate within the temperature region of 0.2–2 GK. Those 21 resonances above $E_r = 1.061$ MeV make only negligible contributions to the total reaction rate up to 2 GK. Therefore, the contributions from the levels presented in Tables 1 and 2 should be adequate to account for these two resonant rates at XRB temperatures.

2.2. Direct-capture Rates

The nonresonant direct-capture (DC) rate for proton capture can be estimated by the following expression (Angulo

Table 2
Properties of ^{66}Se for the Ground-state Capture Utilized in the Present ^{65}As$(p,\gamma)^{66}$Se Resonant Rate Calculation

J_i^{π} [a]	E_x (MeV)		E_r (MeV)[c]	$C^2S_{7/2}$	$C^2S_{3/2}$	$C^2S_{5/2}$	$C^2S_{1/2}$	Γ_γ (eV)	Γ_p (eV)	$\omega\gamma$ (eV)
	$E_x^{\rm exp}$ [b]	$E_x^{\rm theo}$ [a]		($l=3$)	($l=1$)	($l=3$)	($l=1$)			
0_1^+	0.000	0.000	⋯	⋯	0.746	⋯	⋯	⋯	⋯	⋯
2_1^+	0.929(7)	0.982	⋯	0.037	0.069	0.119	0.045	2.765×10^{-4}	⋯	⋯
0_2^+	⋯	1.130	⋯	⋯	0.013	⋯	⋯	2.020×10^{-8}	⋯	⋯
2_2^+	⋯	1.552	⋯	0.002	0.011	0.071	0.051	1.402×10^{-4}	⋯	⋯
0_3^+	⋯	1.575	⋯	⋯	0.002	⋯	⋯	2.056×10^{-6}	⋯	⋯
2_3^+	⋯	1.952	0.232	0.001	0.001	0.180	0.000	4.040×10^{-4}	3.079×10^{-20}	1.924×10^{-20}
0_4^+	⋯	1.989	0.269	⋯	0.002	⋯	⋯	1.441×10^{-8}	4.797×10^{-18}	5.996×10^{-19}
2_4^+	⋯	2.053	0.333[e]	0.002	0.005	0.027	0.025	2.218×10^{-4}	3.517×10^{-14}	2.198×10^{-14}
4_1^+	2.064(3)[d]	2.110	0.344	0.008	⋯	0.004	⋯	8.382×10^{-4}	2.301×10^{-16}	2.589×10^{-16}
3_1^+	⋯	2.102	0.382	0.001	0.000	0.017	⋯	3.835×10^{-5}	1.057×10^{-14}	9.249×10^{-15}
2_5^+	⋯	2.277	0.557[e]	0.000	0.004	0.015	0.001	1.751×10^{-4}	2.205×10^{-9}	1.378×10^{-9}
3_2^+	⋯	2.419	0.699	0.000	0.004	0.063	⋯	2.361×10^{-4}	1.781×10^{-7}	1.557×10^{-7}
1_1^+	⋯	2.474	0.754[e]	⋯	0.016	0.000	0.052	3.579×10^{-3}	1.152×10^{-5}	4.306×10^{-6}
4_2^+	⋯	2.498	0.778	0.001	⋯	0.115	⋯	2.653×10^{-4}	1.888×10^{-7}	2.122×10^{-7}
2_6^+	⋯	2.556	0.836[e]	0.001	0.021	0.033	0.032	9.915×10^{-4}	6.723×10^{-5}	3.935×10^{-5}
3_3^+	⋯	2.668	0.948	0.000	0.065	0.145	⋯	1.550×10^{-4}	7.969×10^{-4}	1.136×10^{-4}
4_3^+	⋯	2.740	1.020	0.002	⋯	0.040	⋯	8.404×10^{-4}	8.287×10^{-6}	9.232×10^{-6}
1_2^+	⋯	2.781	1.061[e]	⋯	0.060	0.351	0.002	5.338×10^{-3}	4.483×10^{-3}	9.137×10^{-4}
2_7^+	⋯	2.865	1.145	0.000	0.000	0.000	0.028	1.175×10^{-3}	5.315×10^{-3}	6.014×10^{-4}
1_3^+	⋯	2.867	1.147	⋯	0.065	0.001	0.222	2.170×10^{-3}	5.887×10^{-2}	7.847×10^{-4}
3_4^+	⋯	2.882	1.162	0.002	0.003	0.002	⋯	1.209×10^{-3}	9.439×10^{-4}	4.639×10^{-4}
0_5^+	⋯	2.888	1.168	⋯	0.629	⋯	⋯	1.716×10^{-4}	1.985×10^{-1}	2.143×10^{-5}
4_4^+	⋯	2.907	1.187	0.000	⋯	0.005	⋯	3.139×10^{-4}	1.001×10^{-5}	1.091×10^{-5}
2_8^+	⋯	2.949	1.229	0.000	0.003	0.005	0.016	9.006×10^{-4}	1.085×10^{-2}	5.197×10^{-4}
3_5^+	⋯	2.969	1.249	0.000	0.006	0.000	⋯	7.804×10^{-4}	4.817×10^{-3}	5.877×10^{-4}
4_5^+	⋯	2.998	1.278	0.000	⋯	0.079	⋯	1.392×10^{-3}	4.711×10^{-4}	3.960×10^{-4}
4_6^+	⋯	3.114	1.394	0.000	⋯	0.157	⋯	1.374×10^{-3}	3.262×10^{-3}	1.088×10^{-3}
2_9^+	⋯	3.217	1.497	0.000	0.003	0.021	0.036	1.534×10^{-3}	3.221×10^{-1}	9.539×10^{-4}
0_6^+	⋯	3.231	1.511	⋯	0.002	⋯	⋯	2.561×10^{-3}	2.244×10^{-2}	2.873×10^{-4}
3_6^+	⋯	3.237	1.517	0.000	0.000	0.006	⋯	1.586×10^{-3}	5.258×10^{-3}	1.066×10^{-3}
1_4^+	⋯	3.274	1.554	⋯	0.005	0.072	0.010	3.113×10^{-3}	2.111×10^{-1}	1.151×10^{-3}
4_7^+	⋯	3.299	1.579	0.000	⋯	0.008	⋯	9.407×10^{-4}	1.075×10^{-3}	5.644×10^{-4}
3_7^+	⋯	3.328	1.608	0.001	0.004	0.022	⋯	1.139×10^{-3}	8.762×10^{-2}	9.842×10^{-4}
2_{10}^+	⋯	3.330	1.610	0.008	0.083	0.001	0.012	2.089×10^{-3}	$2.222 \times 10^{+0}$	1.304×10^{-3}
2_{11}^+	⋯	3.357	1.637	0.001	0.000	0.027	0.114	1.348×10^{-3}	$2.761 \times 10^{+0}$	8.423×10^{-4}
5_1^+	⋯	3.394	1.674	0.000	⋯	⋯	⋯	1.355×10^{-3}	1.460×10^{-4}	1.812×10^{-4}
4_8^+	⋯	3.424	1.704	0.000	⋯	0.018	⋯	1.417×10^{-3}	5.639×10^{-3}	1.274×10^{-3}
3_8^+	⋯	3.487	1.767	0.000	0.000	0.056	⋯	4.881×10^{-3}	2.792×10^{-2}	3.635×10^{-3}
2_{12}^+	⋯	3.499	1.779	0.006	0.060	0.001	0.041	4.335×10^{-4}	$7.440 \times 10^{+0}$	2.709×10^{-4}

Notes.
[a] Calculated by the present shell model.
[b] Measured by Obertelli et al. (2011) and Ruotsalainen et al. (2013).
[c] Calculated by $E_r = E_x - S_p$ with $S_p = 1.720$ MeV (AME2012).
[d] Calculated E_r and Γ_p based on the experimental value of $E_x = 2.064$ MeV for this state.
[e] Resonances dominantly contributing to the rate within temperature region of 0.2–2 GK.

et al. 1999; Schatz et al. 2005).

$$N_A\langle\sigma v\rangle^i_{\rm DC} = 7.83 \times 10^9 \left(\frac{Z_T}{\mu T_9^2}\right)^{1/3} \times S^i_{\rm DC}(E_0) \times \exp\left[-4.249\left(\frac{Z_T^2\mu}{T_9}\right)^{1/3}\right] [\rm cm^3\,s^{-1}\,mol^{-1}], \quad (9)$$

with Z_T being the atomic number of either ^{64}Ge or ^{65}As. The effective astrophysical S-factor at the Gamow energy E_0, i.e., $S^i_{\rm DC}(E_0)$, can be expressed by (Fowler & Hoyle 1964; Rolfs & Rodney 1988),

$$S^i_{\rm DC}(E_0) = S^i(0)\left(1 + \frac{5}{12\tau}\right), \quad (10)$$

where $S^i(0)$ is the S-factor at zero energy, and the dimensionless parameter τ is given numerically by $\tau = 4.2487(Z_T^2\mu/T_9)^{-1/3}$ for the proton capture.

Table 3
Properties of ^{66}Se for the First-excited-state Capture Utilized in the Present ^{65}As$^{5/2^-_1}(p,\gamma)^{66}$Se Resonant Rate

J_i^{π} [a]	E_x (MeV)		E_r (MeV)[c]	$C^2S_{7/2}$ ($l=3$)	$C^2S_{3/2}$ ($l=1$)	$C^2S_{5/2}$ ($l=3$)	$C^2S_{1/2}$ ($l=1$)	Γ_γ (eV)	Γ_p (eV)	$\omega\gamma$ (eV)
	$E_x^{\rm exp}$ [d]	$E_x^{\rm theo}$ [a]								
2_3^+	⋯	1.952	0.045	0.002	0.035	0.000	0.013	4.040×10^{-4}	4.401×10^{-56}	1.834×10^{-56}
0_4^+	⋯	1.989	0.082	⋯	⋯	0.244	⋯	1.441×10^{-8}	2.398×10^{-40}	1.998×10^{-41}
2_4^+	⋯	2.053	0.146	0.000	0.019	0.088	0.098	2.218×10^{-4}	4.499×10^{-26}	1.875×10^{-26}
4_1^+	2.064(3)[d]	2.110	0.157	0.001	0.016	0.002	⋯	8.382×10^{-4}	1.261×10^{-25}	9.458×10^{-26}
3_1^+	⋯	2.102	0.195	0.001	0.011	0.000	0.001	3.835×10^{-5}	4.039×10^{-22}	2.356×10^{-22}
2_5^+	⋯	2.277	0.370	0.001	0.038	0.020	0.184	1.751×10^{-4}	4.549×10^{-12}	1.895×10^{-12}
3_2^+	⋯	2.419[e]	0.512	0.001	0.083	0.004	0.226	2.361×10^{-4}	1.862×10^{-8}	1.086×10^{-8}
1_1^+	⋯	2.474	0.567	0.000	0.000	0.002	⋯	3.579×10^{-3}	5.149×10^{-11}	1.287×10^{-11}
4_2^+	⋯	2.498	0.591	0.000	0.043	0.208	⋯	2.653×10^{-4}	6.133×10^{-8}	4.599×10^{-8}
2_6^+	⋯	2.556	0.649	0.001	0.026	0.191	0.008	9.915×10^{-4}	3.292×10^{-7}	1.371×10^{-7}
3_3^+	⋯	2.668[e]	0.761	0.004	0.107	0.000	0.002	1.550×10^{-4}	2.983×10^{-5}	1.459×10^{-5}
4_3^+	⋯	2.740	0.833	0.002	0.011	0.001	⋯	8.404×10^{-4}	1.353×10^{-5}	9.987×10^{-6}
1_2^+	⋯	2.781	0.874	0.001	0.032	0.002	⋯	5.338×10^{-3}	9.809×10^{-5}	2.408×10^{-5}
2_7^+	⋯	2.865[e]	0.958	0.000	0.002	0.324	0.054	1.175×10^{-3}	6.788×10^{-4}	1.793×10^{-4}
1_3^+	⋯	2.867	0.960	0.000	0.000	0.004	⋯	2.170×10^{-3}	2.502×10^{-7}	6.254×10^{-8}
3_4^+	⋯	2.882[e]	0.975	0.001	0.008	0.001	0.035	1.209×10^{-3}	7.087×10^{-4}	2.607×10^{-4}
0_5^+	⋯	2.888	0.981	⋯	⋯	0.089	⋯	1.716×10^{-4}	8.636×10^{-6}	6.852×10^{-7}
4_4^+	⋯	2.907	1.000	0.000	0.000	0.518	⋯	3.139×10^{-4}	6.881×10^{-5}	4.233×10^{-5}
2_8^+	⋯	2.949	1.042	0.000	0.006	0.012	0.007	9.006×10^{-4}	6.740×10^{-4}	1.606×10^{-4}
3_5^+	⋯	2.969[e]	1.062	0.002	0.003	0.001	0.025	7.804×10^{-4}	1.754×10^{-3}	3.151×10^{-4}
4_5^+	⋯	2.998[e]	1.091	0.003	0.025	0.000	⋯	1.392×10^{-3}	2.795×10^{-3}	6.970×10^{-4}
4_6^+	⋯	3.114[e]	1.207	0.001	0.061	0.103	⋯	1.374×10^{-3}	3.138×10^{-2}	9.872×10^{-4}
2_9^+	⋯	3.217	1.310	0.000	0.019	0.016	0.001	1.534×10^{-3}	3.314×10^{-2}	6.107×10^{-4}
0_6^+	⋯	3.231	1.324	⋯	⋯	0.025	⋯	2.561×10^{-3}	2.545×10^{-4}	1.929×10^{-5}
3_6^+	⋯	3.237	1.330	0.001	0.007	0.000	0.053	1.586×10^{-3}	1.026×10^{-1}	9.112×10^{-4}
1_4^+	⋯	3.274	1.367	0.002	0.002	0.002	⋯	3.113×10^{-3}	4.840×10^{-3}	4.737×10^{-4}
4_7^+	⋯	3.299	1.392	0.000	0.003	0.026	⋯	9.407×10^{-4}	1.039×10^{-2}	6.470×10^{-4}
3_7^+	⋯	3.328	1.421	0.001	0.073	0.003	0.019	1.139×10^{-3}	4.284×10^{-1}	6.629×10^{-4}
2_{10}^+	⋯	3.330	1.423	0.000	0.015	0.036	0.001	2.089×10^{-3}	7.650×10^{-2}	8.473×10^{-4}
2_{11}^+	⋯	3.357	1.450	0.000	0.020	0.001	0.006	1.348×10^{-3}	1.496×10^{-1}	5.568×10^{-4}
5_1^+	⋯	3.394	1.487	0.002	⋯	0.000	⋯	1.355×10^{-3}	$3.592 \times 10^{+3}$	1.242×10^{-3}
4_8^+	⋯	3.424	1.517	0.000	0.013	0.145	⋯	1.417×10^{-3}	1.591×10^{-1}	1.054×10^{-3}
3_8^+	⋯	3.487	1.580	0.000	0.051	0.000	0.001	4.881×10^{-3}	9.800×10^{-1}	2.833×10^{-3}
2_{12}^+	⋯	3.499	1.592	0.001	0.006	0.041	0.008	4.335×10^{-4}	2.659×10^{-1}	1.803×10^{-4}

Notes.
[a] Calculated by the present shell model.
[d] Measured by Obertelli et al. (2011) and Ruotsalainen et al. (2013).
[c] Calculated by $E_r = E_x - S_p - 0.187$ in units of MeV, with $S_p = 1.720$ MeV (AME2012).
[d] Calculated E_r and Γ_p based on the experimental value of $E_x = 2.064$ MeV for this state.
[e] Resonances dominantly contributing to the rate within temperature region of 0.2–2 GK.

In this work, we have calculated the DC S-factors with the RADCAP code (Bertulani 2003). The Woods–Saxon nuclear potential (central + spin orbit) and a Coulomb potential of uniform-charge distribution were utilized in the calculation. The nuclear central potential V_0 was determined by matching the bound-state energies. The spectroscopic factors were taken from the shell model calculation and are listed in Table 1 and Table 2. The optical-potential parameters (Huang et al. 2010) are $R_0 = R_{\rm s.o.} = R_C = 1.25 \times (1 + A_T)^{1/3}$ fm, $a_0 = a_{\rm s.o.} = 0.65$ fm, with a spin-orbit potential depth of $V_{\rm s.o.} = -10$ MeV. Here, R_0, $R_{\rm s.o.}$, and R_C are the radii of central potential, the spin-orbit potential and the Coulomb potential, respectively; a_0 and $a_{\rm s.o.}$ are the corresponding diffuseness parameters in the central and spin-orbit potentials, respectively.

For the ^{65}As$(p,\gamma)^{66}$Se reaction, $S(0)$ values for DC captures into the ground state and the first-excited state ($E_x = 929$ keV) in ^{66}Se are calculated to be 8.3 and 3.5 MeV·b, respectively. The total DC rate for this reaction is only about 0.1% that of the resonant one at 0.05 GK. For the ^{64}Ge$(p,\gamma)^{65}$As reaction, we find a DC $S(0)$ value for this reaction of about 35 MeV·b. The DC contribution is only about 0.3% even at the lowest temperature of 0.06 GK. Even when considering estimated upper limits to the DC contribution (He et al. 2014), the resonant contributions still dominate the total rates above 0.06 GK and 0.05 GK for ^{64}Ge$(p,\gamma)^{65}$As and ^{65}As$(p,\gamma)^{66}$Se reactions, respectively. The probabilities of populating the first-excited states in ^{64}Ge ($E_x = 902$ keV) and ^{65}As ($E_x = 187$ keV) relative to the ground states at temperatures below 0.1 GK are extremely small, and hence contributions of the direct-capture from these excited states can be neglected.

Table 4
Thermonuclear ^{64}Ge(p,γ)^{65}As and ^{65}As(p,γ)^{66}Se Rates in Units of cm^3 s^{-1} mol^{-1}

	^{64}Ge(p,γ)^{65}As			^{65}As(p,γ)^{66}Se		
T_9	$N_A\langle\sigma v\rangle$	Lower	Upper	$N_A\langle\sigma v\rangle$	Lower	Upper
0.2	4.79×10^{-17}	3.99×10^{-20}	1.23×10^{-15}	1.86×10^{-16}	9.97×10^{-18}	1.45×10^{-15}
0.3	1.33×10^{-13}	8.44×10^{-15}	7.66×10^{-13}	2.21×10^{-12}	1.79×10^{-12}	1.92×10^{-11}
0.4	3.08×10^{-11}	9.92×10^{-13}	6.56×10^{-11}	1.96×10^{-9}	8.15×10^{-10}	8.26×10^{-9}
0.5	1.89×10^{-9}	1.98×10^{-10}	4.30×10^{-9}	1.51×10^{-7}	3.03×10^{-8}	4.65×10^{-7}
0.6	5.47×10^{-8}	1.42×10^{-8}	8.93×10^{-8}	3.08×10^{-6}	3.31×10^{-7}	7.55×10^{-6}
0.7	6.86×10^{-7}	2.61×10^{-7}	9.38×10^{-7}	2.93×10^{-5}	1.73×10^{-6}	5.91×10^{-5}
0.8	4.62×10^{-6}	2.15×10^{-6}	6.52×10^{-6}	1.69×10^{-4}	6.47×10^{-6}	2.94×10^{-4}
0.9	2.02×10^{-5}	8.05×10^{-6}	3.52×10^{-5}	6.86×10^{-4}	2.18×10^{-5}	1.08×10^{-3}
1.0	6.53×10^{-5}	2.17×10^{-5}	1.39×10^{-4}	2.15×10^{-3}	7.04×10^{-5}	3.19×10^{-3}
1.1	1.69×10^{-4}	4.69×10^{-5}	4.30×10^{-4}	5.55×10^{-3}	2.12×10^{-4}	7.96×10^{-3}
1.2	3.69×10^{-4}	8.83×10^{-5}	1.09×10^{-3}	1.23×10^{-2}	4.67×10^{-4}	1.74×10^{-2}
1.3	7.10×10^{-4}	1.50×10^{-4}	2.38×10^{-3}	2.42×10^{-2}	9.89×10^{-4}	3.41×10^{-2}
1.4	1.24×10^{-3}	2.34×10^{-4}	4.62×10^{-3}	4.33×10^{-2}	1.90×10^{-3}	6.11×10^{-2}
1.5	1.98×10^{-3}	3.42×10^{-4}	8.16×10^{-3}	7.18×10^{-2}	3.33×10^{-3}	1.02×10^{-1}
1.6	2.98×10^{-3}	4.73×10^{-4}	1.33×10^{-2}	1.12×10^{-1}	5.69×10^{-3}	1.59×10^{-1}
1.7	4.25×10^{-3}	6.28×10^{-4}	2.04×10^{-2}	1.65×10^{-1}	9.38×10^{-3}	2.34×10^{-1}
1.8	5.78×10^{-3}	8.02×10^{-4}	2.97×10^{-2}	2.34×10^{-1}	1.49×10^{-2}	3.31×10^{-1}
1.9	7.58×10^{-3}	9.93×10^{-4}	4.13×10^{-2}	3.18×10^{-1}	2.22×10^{-2}	4.50×10^{-1}
2.0	9.63×10^{-3}	1.20×10^{-3}	5.52×10^{-2}	4.19×10^{-1}	3.21×10^{-2}	5.93×10^{-1}

3. RESULTS

The resulting total thermonuclear ^{64}Ge(p,γ)^{65}As and ^{65}As(p,γ)^{66}Se rates are listed in Table 4 as a function of temperature. The present (*Present*, hereafter) rates can be parameterized by the standard format of Rauscher & Thielemann (2000). For ^{64}Ge(p, γ)^{65}As, we find

$$N_A\langle\sigma v\rangle = \exp\left(-78.204 - \frac{13.819}{T_9} + \frac{12.211}{T_9^{1/3}} + 81.566T_9^{1/3} - 13.138T_9 + 1.717T_9^{5/3} - 16.149\ln T_9\right) + \exp\left(-93.260 - \frac{10.059}{T_9} + \frac{15.189}{T_9^{1/3}} + 61.887T_9^{1/3} + 21.717T_9 - 8.625T_9^{5/3} - 22.943\ln T_9\right) + \exp\left(-75.104 - \frac{3.788}{T_9} + \frac{19.347}{T_9^{1/3}} + 52.700T_9^{1/3} - 32.227T_9 + 14.766T_9^{5/3} + 1.270\ln T_9\right),$$

with a fitting error of less than 0.3% at 0.1–2 GK; for ^{65}As(p, γ)^{66}Se, we find

$$N_A\langle\sigma v\rangle = \exp\left(-111.177 - \frac{2.639}{T_9} + \frac{50.997}{T_9^{1/3}} + 106.669T_9^{1/3}. - 64.623T_9 + 13.521T_9^{5/3} + 31.256\ln T_9\right) + \exp\left(-124.702 - \frac{12.436}{T_9} + \frac{52.765}{T_9^{1/3}} + 89.593T_9^{1/3} - 12.219T_9 + 0.456T_9^{5/3} - 2.886\ln T_9\right) + \exp\left(-116.814 - \frac{5.202}{T_9} + \frac{63.424}{T_9^{1/3}} + 48.281T_9^{1/3}. + 83.320T_9 - 188.849T_9^{5/3} + 21.362\ln T_9),\right)$$

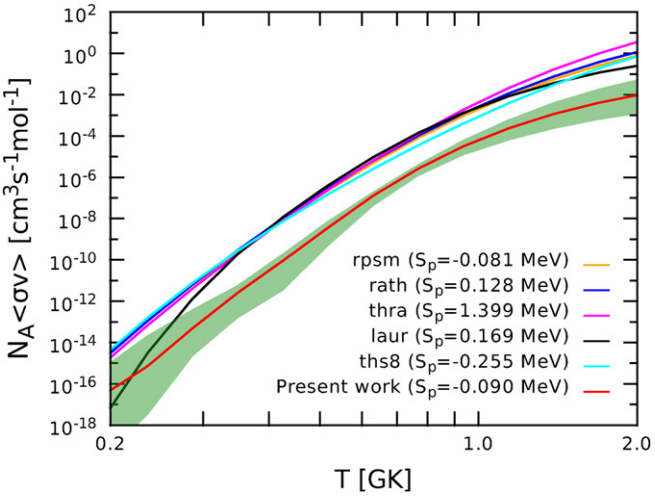

Figure 1. Reaction rates of the ^{64}Ge(p,γ)^{65}As reaction (in units of cm^3 mol^{-1} s^{-1}). The *Present* rate (red line) together with the upper and lower limits deduced from uncertainties are shown by a (green) colored band. Other available rates from JINA REACLIB (Cyburt et al. 2010) are shown for comparison. See details in the text and Table 4.

with a fitting error of less than 0.4% at 0.1–2 GK. We emphasize that the above fits are only valid with the stated error over the temperature range of 0.1–2 GK. Above 2 GK, one may, for example, match our rates to statistical model calculations (see, e.g., NACRE by Angulo et al. 1999).

Figure 1 shows the comparison of the *Present* ^{64}Ge(p,γ)^{65}As rate with others compiled in JINA REACLIB: *rpsm*, *rath*, *thra*, *laur*, and *ths8*. Note that only the *rpsm* rate uses an S_p(^{65}As) value that is within 1σ of the recently determined experimental value. The *Present* rate differs significantly from others in the temperature region of interest in XRBs. The disagreement, particularly with the *rpsm* rate, demonstrates that the statistical model is not applicable for this reaction owing to the low density of excited states in ^{65}As.

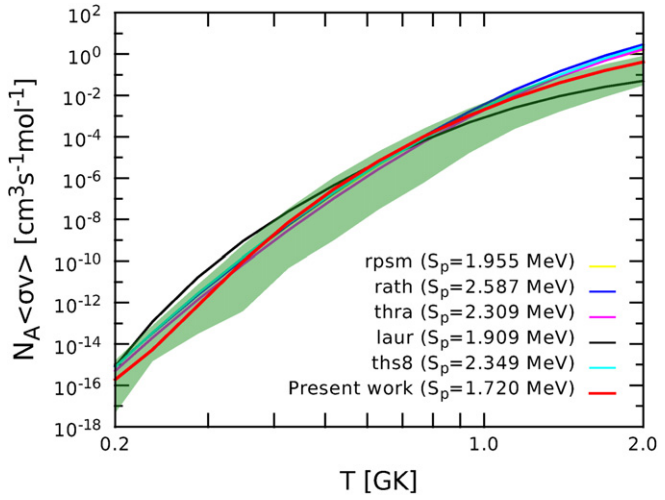

Figure 2. Same as Figure 1, but for the ^{65}As$(p,\gamma)^{66}$Se reaction. Note that the *rpsm* rate is quite close to the *rath*, *ths8,* and *thra* rates at different temperature regions (Cyburt et al. 2010), and hence the corresponding line is not clearly visible. See details in the text and Table 4.

Similarly, the comparison of the *Present* ^{65}As$(p,\gamma)^{66}$Se rate with other rates available in the JINA REACLIB: *rpsm*, *rath*, *thra*, *laur*, and *ths8*, is presented in Figure 2. Only the *laur* and *rpsm* rates use $S_p(^{66}\mathrm{Se})$ values that are within 1σ of the currently accepted value. Although the *Present* rate differs significantly from the others, especially at lower and higher temperature regions, it is consistent with all others within the remaining large uncertainties. At $T > 1$ GK, the *laur* rate is the lowest rate simply because only three excited states were considered by Van Wormer et al. (1994). It should be noted that the shell model calculation provides the first reliable estimate of the uncertainty of the ^{65}As(p,γ) reaction rate, especially as the Hauser-Feshbach rates may suffer from unknown systematic errors due to the limited applicability of the statistical model near the proton drip line.

Uncertainties for the *Present* ^{64}Ge$(p,\gamma)^{65}$As and ^{65}As$(p,\gamma)^{66}$Se rates were estimated by considering the uncertainties in the S_p values ($\pm$85 keV for ^{65}As and $\pm$310 keV for ^{66}Se) and estimated uncertainties in the calculated level energies ($\pm$168 keV for both ^{65}As and ^{66}Se (Honma et al. 2002)[7]). These were added in quadrature to give uncertainties of $\pm$188 keV and $\pm$353 keV for the resonance energies E_r of ^{64}Ge$(p,\gamma)^{65}$As and ^{65}As$(p,\gamma)^{66}$Se, respectively. Note that for the two known levels, i.e., $E_x = 187$ keV in ^{65}As and $E_x = 2064$ keV in ^{66}Se, an experimental excitation energy uncertainty of $\pm$3 keV is used instead. For ^{64}Ge$(p,\gamma)^{65}$As, all resonance strengths $\omega\gamma$ are proportional to Γ_p since $\Gamma_p \ll \Gamma_\gamma$ (see Table 1 and Equation (3)). The uncertainties in Γ_p (or $\omega\gamma$) owing to the uncertainties in E_r are calculated based on the energy dependence expressed in Equation (5). In the case of ^{65}As$(p,\gamma)^{66}$Se, only five resonances (at $E_r = 0.333$, 0.557, 0.754, 0.836, and 1.061 MeV dominate the resonant rate within the temperature region of 0.2–2 GK. Here, the resonant strengths $\omega\gamma$ are proportional to Γ_p for the first four resonances, while the strength of the last resonance at 1.061 MeV (dominating over ~0.9–2 GK) depends on both, Γ_p and Γ_γ. Uncertainties in Γ_γ can be neglected because of the much larger rate uncertainties caused by E_r and Γ_p. The uncertainties for all resonances listed in Table 2 are considered in the present calculations.

[7] The ^{66}Zn case is studied with the present model space and interaction, and an rms deviation between the experimental and calculated level energies is found to be about 140 keV (Y. H. Lam et al. 2016, in preparation).

4. ASTROPHYSICAL IMPLICATIONS

We examine the impact of our new ^{64}Ge(p,γ) and ^{65}As(p,γ) rates and their uncertainties on the *rp*-process using one-zone XRB models. Post processing calculations using temperature and density trajectories from the literature enable a quick assessment of the impact of nuclear physics changes on the strength of the ^{64}Ge waiting point using the $A = 64$ abundance, and on the burst energy generation rate. We use the post-processing approach for the K04 XRB model (Parikh et al. 2008, 2009). However, post-processing calculations do not take into account the changes in temperature and density that result from the energy generation changes. Therefore, they cannot reliably predict the quantitative impact on produced abundances and light curves. To account for this effect, we also use the full one-zone XRB model (Schatz et al. 2001), which represents a more extreme burst with very hydrogen rich ignition.

4.1. Post Processing Results for K04

With the representative K04 thermodynamic history (Parikh et al. 2008, 2009), final abundances (as mass fractions X) and the nuclear energy generation rate E_{gen} during a burst have been studied by performing separate XRB model calculations with different rates. In the K04 model, the peak temperature $T_{\mathrm{peak}} = 1.4$ GK is similar to those reached at the base of the envelope in comparable hydrodynamic XRB models (e.g., 1.3 GK in José et al. 2010). Figures 3 and 4 compare results for X and E_{gen} using rates from the present work to results using rates available in JINA REACLIB: *laur, rath, rpsm, thra, ths8*. The impact of (a) using different ^{64}Ge(p,γ) rates (with the ^{65}As(p,γ) rate held constant at the *Present* value), (b) using different ^{65}As(p,γ) rates (with the ^{64}Ge(p,γ) rate held constant at the *Present* value), and (c) using different ^{64}Ge(p,γ) and ^{65}As(p,γ) rates together, is indicated in each of the two figures. For each change in reaction rate, the corresponding inverse reaction rate is also changed to maintain detailed balance. This inverse rate strongly depends on the adopted reaction S_p-value for the respective forward rate. As we compare the impact of different rates that have been determined using very different S_p values (see Section 2 and Figures 1 and 2), the results illustrate not only the influence of the rate calculation, but also the influence of different forward to reverse rate ratios due to different S_p-values.

The results of Figures 3 and 4 are interesting, but not entirely unexpected. For the case of the ^{64}Ge(p,γ) reaction, an equilibrium between the rates of the forward (p,γ) and reverse (γ,p) processes is quickly established due to the small (p,γ) Q-value relative to kT at XRB temperatures: at 1 GK, $kT \approx 100$ keV. As a result, it is the (p,γ) Q-value, rather than the actual ^{64}Ge(p,γ) rate, that is the most important nuclear physics quantity needed to characterize the equilibrium abundance of ^{65}As (and the subsequent flow of material to heavier nuclei through the ^{65}As(p,γ) reaction); see Schatz et al. (1998), Iliadis (2007), Parikh et al. (2009). This is nicely illustrated in Figure 3(a): the ^{64}Ge(p,γ) rates adopting positive (p,γ) Q-values (*thra, laur, rath*) give relatively lower final abundances around $A = 64$ and larger abundances at higher

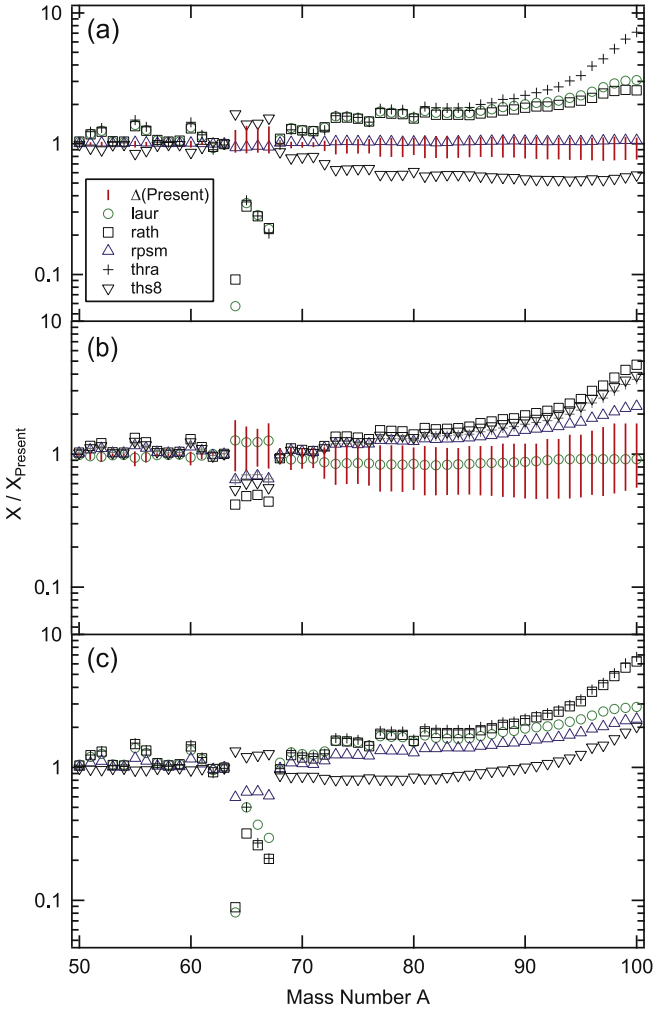

Figure 3. Final abundances, as mass fractions X, following one-zone XRB calculations using the K04 thermodynamic history (Parikh et al. 2008, 2009). Results using rates determined in the *Present* work and in JINA REACLIB: *rpsm*, *rath*, *thra*, *laur*, and *ths8* are indicated. Panels (a) and (b) show the effects of using either different ^{64}Ge(p,γ) or different ^{65}As(p,γ) rates, respectively, while panel (c) shows the effect of using different ^{64}Ge(p,γ) and ^{65}As(p,γ) rates together. The impact of the uncertainties in the *Present* ^{64}Ge(p,γ) and ^{65}As(p,γ) rates (see Figures 1 and 2) is indicated as Δ *(Present)* in panels (a) and (b).

masses precisely because of the larger equilibrium abundances of ^{65}As during the burst, allowing for increased flows of abundances to higher masses via the ^{65}As(p,γ) reaction. On the other hand, the opposite is true for those rates adopting negative (p,γ) Q-values (*ths8, Present, rpsm*) because of the larger equilibrium abundances of ^{64}Ge and lower relative abundances of ^{65}As during the burst. Indeed, the summed mass fractions of species with $A > 70$, X_{70}, vary considerably for different choices of Q-values. For example, when the *thra*, *ths8*, or *Present* rates are adopted, $X_{70} = 0.58$, 0.21, or 0.33, respectively.

A consequence of the increased flow of abundances to heavier nuclei is seen in Figure 4(a), where the models adopting the *thra, laur*, and *rath* rates give the largest $E_{\rm gen}$ at late times due to energy released from the decay of the larger amounts of heavy nuclei produced during the burst. As expected, the opposite is true for $E_{\rm gen}$ in the models using the *ths8, Present*, and *rpsm* rates. We note that the predictions for $E_{\rm gen}$ at late times vary rather significantly between the models using the different rates, with differences as large as a factor of ≈2.

For the case of the ^{65}As(p,γ) reaction, where a large positive (p,γ) Q-value is adopted in all rate estimates, the importance of the actual rate is illustrated in Figure 3(b). The model adopting the largest rate at the most relevant temperatures ($T > 0.9$ GK, see José et al. 2010), *rath*, gives the lowest abundances around $A = 64$ and the largest abundances at higher masses. Again, as expected, the opposite is true for the model using the lowest ^{65}As(p,γ) rate, *laur*. The variation in X_{70} for different choices of the ^{65}As(p,γ) rate is significant, with $X_{70} = 0.49$ with the *rath* rate, and 0.29 with the *laur* rate. The behavior of $E_{\rm gen}$ for these models is again in accordance with the distributions of the final abundances, with the largest $E_{\rm gen}$ at late times arising from the model using the *rath* rate, and the lowest $E_{\rm gen}$ arising from the model using the *laur* rate.

Finally, the effects of using different ^{64}Ge(p,γ) and ^{65}As(p,γ) rates from the same theoretical model calculation are shown in Figures 3(c) and 4(c). This reveals the impact of competing influences from these two rates. For example, the model using the *ths8* ^{64}Ge(p,γ) rate gave the lowest relative abundances at higher masses (see Figure 3(a)), while the model using the *ths8* ^{65}As(p,γ) rate gave among the highest relative abundances at higher masses (see Figure 3(b)). When these two rates are used together, the combined impact on the final abundances (and $E_{\rm gen}$) is, not surprisingly, moderated.

Figure 3(c) also shows that using the *Present* ^{64}Ge(p,γ) and ^{65}As(p,γ) rates results in the strongest ^{64}Ge waiting point, and the lowest final abundances at the highest masses. Differences with respect to predictions using rates from JINA REACLIB are as large as a factor of ≈7 at individual values of A. X_{70} calculated with the two *Present* rates differs by as much as factor of 1.8 from models using the other rates.

We have also examined the impact on XRB model predictions of our uncertainties in the *Present* ^{64}Ge(p,γ) and ^{65}As(p,γ) rates, as shown in Figures 1 and 2. Reverse rates for the lower and upper forward rates were determined using exactly the Q-values adopted for the corresponding forward rate calculations. Panels (a) and (b) of Figures 3 and 4 show how these rate uncertainties affect final abundances and $E_{\rm gen}$ in the K04 model, with mass fractions above $A = 64$ varying by up to a factor of three due to the individual uncertainties in the rates, X_{70} varying by up to a factor of two, and $E_{\rm gen}$ varying by up to 35% at late times. The impact on X and $E_{\rm gen}$ of the uncertainties in the *Present* rates is somewhat smaller than that from different choices of rates, but clearly not insignificant. As such, the mass of ^{66}Se should be determined experimentally and the uncertainty in the mass of ^{65}As should be reduced to better constrain model predictions.

4.2. One-zone XRB Model Results

In addition, we explored the impact of the remaining nuclear physics uncertainties related to the ^{64}Ge waiting point on the full one-zone XRB model described in Schatz et al. (2001). We note that this model is different from K04. It represents a burst that ignites in a very hydrogen rich environment, for example at high accretion rates and very low accreted metallicity, and was developed to explore the maximum extent of the *rp*-process toward heavy elements. To determine the total remaining uncertainty in the burst model due to the nuclear physics of the ^{64}Ge waiting point, we performed two extreme calculations. The calculations assume the most favorable (unfavorable)

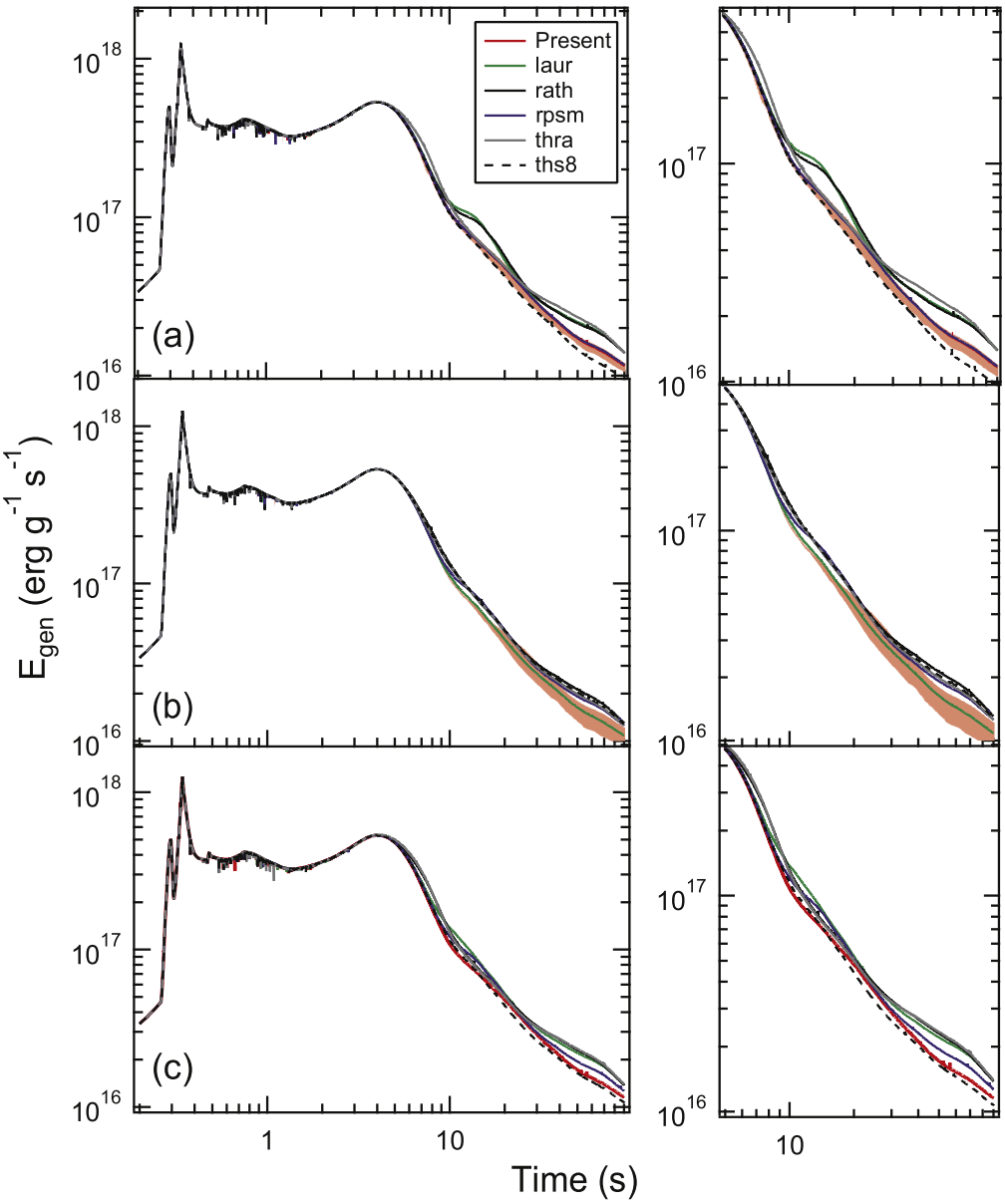

Figure 4. Same as Figure 3, but for nuclear energy generation rates E_{gen} during the burst in the K04 XRB model. Panels (a) and (b) show the effects of using either different ^{64}Ge(p,γ) or different ^{65}As(p,γ) rates, respectively, while panel (c) shows the effect of using different ^{64}Ge(p,γ) and ^{65}As(p,γ) rates together. The impact of the uncertainties in the *Present* ^{64}Ge(p,γ) and ^{65}As(p,γ) rates (see Figures 1 and 2) is indicated in panels (a) and (b). Panels to the right show expanded views of the panels to the left.

nuclear physics choice for the *rp*-process to pass through the ^{64}Ge waiting point, adopting the upper (lower) limit of the ^{64}Ge (p,γ) and ^{65}As(p,γ) reaction rates, and the upper (lower) limits of S_p(^{65}As) and S_p(^{66}Se). Varying S_p values independently, rather than varying individual masses, is justified because the uncertainties in S_p(^{65}As) and S_p(^{66}Se) are each completely dominated by the mass uncertainty of ^{65}As and ^{66}Se, respectively. Figures 5 and 6 show the impact of the nuclear physics uncertainties on burst light curve and final composition. Clearly the nuclear physics uncertainties have a strong impact on observables. The abundance ratio of $A = 64$ to $A = 68$, a measure for the strength of the ^{64}Ge waiting point varies from 1.1 (making ^{64}Ge the strongest waiting point) to 0.2 (making ^{64}Ge not a significant waiting point). This is consistent with the result from Tu et al. (2011) who found that with their new ^{65}As mass ^{64}Ge is only a weak waiting point. However, as we show here, when taking into account all nuclear physics uncertainties, a strong ^{64}Ge waiting point cannot be ruled out. Figure 7 shows the ratio of the final abundances. Similar to the results obtained for model K04 using post-processing, a weak ^{64}Ge waiting point (low ^{64}Ge abundance) leads to an enhancement of the production of heavier elements by up to a factor of two. As already noted by Tu et al. (2011), the production of the heaviest nuclei with $A \geqslant 106$ is, however, reduced for a weak ^{64}Ge waiting point. This somewhat counter intuitive result is a consequence of the faster burning at higher temperature, which leads to a shorter burst as hydrogen is consumed more quickly. This effect is not seen in the post-processing calculation because there the temperature trajectory is fixed.

We also investigated the relative contributions of the various nuclear physics uncertainties. Similar to the K04 post-

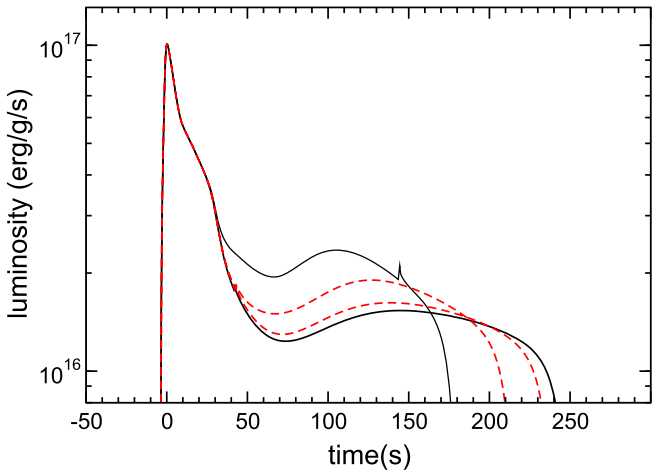

Figure 5. Luminosity per gram of material calculated with the one-zone X-ray burst model for nuclear physics input that, within uncertainties, maximally favors (initially high solid line) and maximally disfavors (initially low solid line) the *rp*-process flow through the ^{64}Ge waiting point. The dashed lines show the results when only the ^{65}As(p,γ) reaction rate is changed within uncertainties, and all other nuclear physics input is fixed.

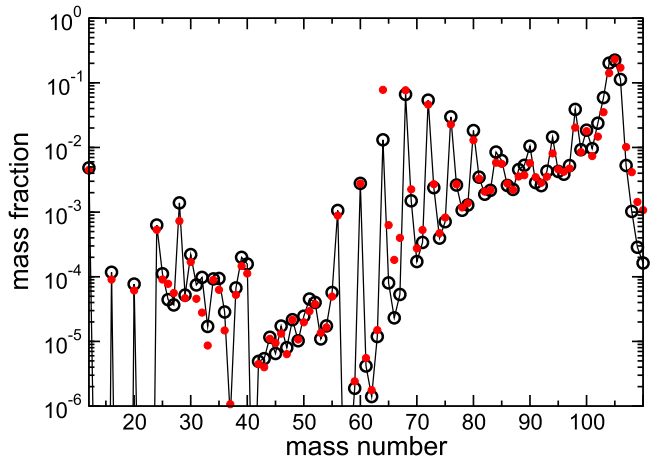

Figure 6. Final mass fractions, summed by mass number, calculated with the one-zone X-ray burst model for nuclear physics input that, within uncertainties, maximally favors (open black circles, solid line) and maximally disfavors (filled red circles) the *rp*-process flow through the ^{64}Ge waiting point.

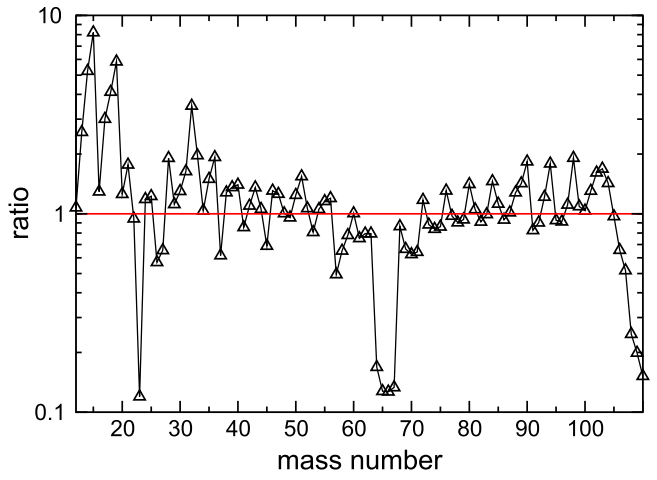

Figure 7. Ratio of the final mass fractions shown in Figure 6.

processing results, we find that the ^{64}Ge(p,γ) reaction rate itself, for a fixed Q-value, has no influence on the burst model due to (p,γ)-(γ,p) equilibrium between ^{64}Ge and ^{65}As. A calculation where only S_p(^{65}As) and S_p(^{66}Se) changes produced virtually the same result as the full variation, demonstrating that the mass uncertainties currently dominate. Changing each S_p separately indicates that the 85 keV uncertainty of S_p(^{65}As) due to the ^{65}As mass uncertainty, and the 310 keV uncertainty of S_p(^{66}Se) mainly due to the unknown ^{66}Se mass contribute roughly equally. However, varying the ^{65}As(p,γ) reaction rate within our new uncertainties, while leaving S_p(^{65}As) and S_p(^{66}Se) fixed at their nominal values, still led to significant light curve changes (see Figure 5) and a change of the $A = 64$ to $A = 68$ ratio from 1 to 0.7. This shows that once the mass uncertainties are addressed, the ^{65}As(p,γ) reaction rate uncertainty will still play a role (even though fixing S_p(^{66}Se) will reduce the rate uncertainty somewhat).

5. SUMMARY AND CONCLUSION

We have determined new thermonuclear rates for the ^{64}Ge(p,γ)^{65}As and ^{65}As(p,γ)^{66}Se reactions based on large-scale shell model calculations and proton separation energies for ^{65}As and ^{66}Se derived using measured masses and, for ^{66}Se, the AME2012 extrapolation. These rates differ strongly from other rates available in the literature. For example, at ≈1 GK, our ^{64}Ge(p,γ) rate is up to a factor of ≈90 lower than other rates, while our ^{65}As(p,γ) rate differs by up to a factor of ≈3 from other rates.

We also determined for the first time reliable uncertainties for the ^{64}Ge(p,γ)^{65}As and ^{65}As(p,γ)^{66}Se reactions. We find that in two different XRB models, the remaining uncertainties in S_p(^{65}As), S_p(^{66}Se), and the ^{65}As(p,γ) reaction rate lead to large uncertainties in the strength of the ^{64}Ge waiting point in the *rp*-process, the produced amount of $A = 64$ material in the burst ashes that will ultimately decay to ^{64}Zn, the produced amount of heavier nuclei beyond $A = 64$, and the burst light curve. These effects are robust and appear in two different XRB models. We conclude that to address these uncertainties a more precise measurement of the ^{65}As mass, a measurement of the ^{66}Se mass, and a measurement of the excitation energies of states in ^{66}Se that serve as important resonances for the ^{65}As(p,γ)^{66}Se reaction will be important.

This work was financially supported by the National Natural Science Foundation of China (Nos. 11490562, 11135005, 11321064, U1432125, U1232208), and the Major State Basic Research Development Program of China (2013CB834406). Y. H.L. gratefully acknowledges financial support from the Ministry of Science and Technology of China (Talented Young Scientist Program) and from the China Postdoctoral Science Foundation (2014M562481). A.P. was supported by the Spanish MICINN under grant No. AYA2013-42762. H.S. was supported by the US National Science Foundation under grant No. PHY-1430152 (JINA Center for the Evolution of the Elements) and PHY 11-02511. B.A.B. was supported by US NSF PHY-1404442.

REFERENCES

Angulo, C., Arnould, M., Rayet, M., et al. 1999, NuPhA, 656, 3
Audi, G., Kondev, F. G., Wang, M., et al. 2012, ChPhC, 36, 1157
Audi, G., & Wapstra, A. H. 1995, NuPhA, 595, 409
Bertulani, C. A. 2003, CoPhC, 156, 123

Brown, B. A. 2014, WSPOT code, http://www.nscl.msu.edu/~brown/reaction-codes/home.html
Brown, B. A., Clement, R. R. C., Schatz, H., Volya, A., & Richter, W. A. 2002, PhRvC, 65, 045802
Brown, B. A., & Rae, W. D. M. 2014, NDS, 120, 115
Browne, E., & Tuli, J. K. 2010, NDS, 111, 2425
Brussaard, P. J., & Glaudemans, P. W. M. 1977, Shell Model Applications in Nuclear Spectroscopy (Amsterdam: North-Holland)
Clark, J. A., Sharma, K. S., Savard, G., et al. 2007, PhRvC, 75, 032801
Cyburt, R. H., Amthor, A. M., Ferguson, R., et al. 2010, ApJS, 189, 240
Elomaa, V.-V., Vorobjev, G. K., Kankainen, A., et al. 2009, PhRvL, 102, 252501
Fisker, J. L., Schatz, H., & Thielemann, F.-K. 2008, ApJS, 174, 261
Fowler, W. A., & Hoyle, F. 1964, ApJS, 9, 201
He, J. J., Parikh, A., Brown, B. A., et al. 2014, PhRvC, 89, 035802
Herndl, H., Görres, J., Wiescher, M., Brown, B. A., & Van Wormer, L. 1995, PhRvC, 52, 1078
Honma, M., Otsuka, T., Brown, B. A., & Mizusaki, T. 2002, PhRvC, 65, 061301R
Honma, M., Otsuka, T., Brown, B. A., & Mizusaki, T. 2004, PhRvC, 69, 034335
Honma, M., Otsuka, T., Brown, B. A., & Mizusaki, T. 2005, EPJA, 25, 499
Huang, J. T., Bertulani, C. A., & Guimarães, V. 2010, ADNDT, 96, 824
Iliadis, C. 2007, Nuclear Physics of Stars (Weinheim: Wiley)
José, J., Moreno, F., Parikh, A., & Iliadis, C. 2010, ApJS, 189, 204
Lewin, W. H. G., Van Paradijs, J., & Taam, R. E. 1993, SSRv, 62, 223
Möller, P., Nix, J. R., Myers, W. D., & Swiatecki, W. J. 1995, ADNDT, 59, 185
Obertelli, A., Baugher, T., Bazin, D., et al. 2011, PhLB, 701, 417
Parikh, A., José, J., Iliadis, C., Moreno, F., Rauscher, T., et al. 2009, PhRvC, 79, 045802
Parikh, A., José, J., Moreno, F., & Iliadis, C. 2008, ApJS, 178, 110
Parikh, A., José, J., & Sala, G. 2014, AIPA, 4, 041002
Parikh, A., José, J., Sala, G., & Iliadis, C. 2013, PrPNP, 69, 225
Pearson, J. M., Nayak, R. C., & Goriely, S. 1996, PhLB, 387, 455
Rauscher, T., & Thielemann, F.-K. 1998, in Stellar Evolution, Stellar Explosions and Galactic Chemical Evolution, ed. A. Mezzacappa (Bristol: IOP), 519
Rauscher, T., & Thielemann, F.-K. 2000, ADNDT, 75, 1
Richter, W. A., Brown, B. A., Signoracci, A., & Wiescher, M. 2011, PhRvC, 83, 065803
Rolfs, C. E., & Rodney, W. S. 1988, Cauldrons in the Cosmos (Chicago: Univ. Chicago Press)
Ruotsalainen, P., Jenkins, D. G., Bentley, M. A., et al. 2013, PhRvC, 88, 041308
Schatz, H. 2006, IJMSp, 251, 293
Schatz, H., Aprahamian, A., Barnard, V., et al. 2001, PhRvL, 86, 3471
Schatz, H., Aprahamian, A., Görres, J., et al. 1998, PhR, 294, 167
Schatz, H., Bertulani, C. A., Brown, B. A., et al. 2005, PhRvC, 72, 065804
Schury, P., Bachelet, C., Block, M., et al. 2007, PhRvC, 75, 055801
Strohmayer, T. E., & Bildsten, L. 2006, in Compact Stellar X-ray Sources, ed. W. Lewin, & M. van der Klis (Cambridge: Cambridge Univ. Press), 113
Tu, X. L., Xu, H. S., Wang, M., et al. 2011, PhRvL, 106, 112501
Van Wormer, L., Görres, J., Iliadis, C., Wiescher, M., & Thielemann, F.-K. 1994, ApJ, 432, 326
Wallace, R. K., & Woosley, S. E. 1981, ApJS, 45, 389
Wang, M., Audi, G., Wapstra, A. H., et al. 2012, ChPhC, 80, 1603
Woosley, S. E., Heger, A., Cumming, A., et al. 2004, ApJS, 151, 75
Xia, J. W., Zhan, W. L., Wei, B. W., et al. 2002, NIMPA, 488, 11